



LAWRENCE  
LIVERMORE  
NATIONAL  
LABORATORY

# Experimental characterization of a strongly coupled solid density plasma generated in a short-pulse laser target interaction

G. Gregori, S. B. Hansen, M. H. Key, J. King, A. J. Mackinnon, H.-S. Park, P. K. Patel, R. Shepard, R. A. Snavely, S. C. Wilks, S. H. Glenzer

April 5, 2005

Contributions of Plasma Physics

## **Disclaimer**

---

This document was prepared as an account of work sponsored by an agency of the United States Government. Neither the United States Government nor the University of California nor any of their employees, makes any warranty, express or implied, or assumes any legal liability or responsibility for the accuracy, completeness, or usefulness of any information, apparatus, product, or process disclosed, or represents that its use would not infringe privately owned rights. Reference herein to any specific commercial product, process, or service by trade name, trademark, manufacturer, or otherwise, does not necessarily constitute or imply its endorsement, recommendation, or favoring by the United States Government or the University of California. The views and opinions of authors expressed herein do not necessarily state or reflect those of the United States Government or the University of California, and shall not be used for advertising or product endorsement purposes.

# Experimental characterization of a strongly coupled solid density plasma generated in a short-pulse laser target interaction

G. Gregori<sup>\*1</sup>, S. B. Hansen<sup>1</sup>, M. H. Key<sup>1</sup>, J. King<sup>1,2</sup>, A. J. Mackinnon<sup>1</sup>, H.-S. Park<sup>1</sup>, P. K. Patel<sup>1</sup>, R. Shepherd<sup>1</sup>, R. A. Snively<sup>1</sup>, S. C. Wilks<sup>1</sup>, and S. H. Glenzer<sup>1</sup>

<sup>1</sup> Lawrence Livermore National Laboratory, University of California, P.O. Box 808, CA 94551

<sup>2</sup> Department of Applied Science, University of California, Davis, CA 95616

We have measured high resolution copper  $K\alpha$  spectra from a picosecond high intensity laser produced plasma. By fitting the shape of the experimental spectra with a self-consistent-field model which includes all the relevant line shifts from multiply ionized atoms, we are able to infer time and spatially averaged electron temperatures ( $T_e$ ) and ionization state ( $Z$ ) in the foil. Our results show increasing values for  $T_e$  and  $Z$  when the overall mass of the target is reduced. In particular, we measure temperatures in excess of 200 eV with  $Z \sim 13$ -14. For these conditions the ion-ion coupling constant is  $\Gamma_{ii} \sim 8$ -9, thus suggesting the achievement of a strongly coupled plasma regime.

Copyright line will be provided by the publisher

## 1 Introduction

Strongly coupled plasma conditions, where the average kinetic energy per electron is comparable to or less than the relative Coulomb interaction among charged particles, are of significant interest in inertial confinement fusion (ICF) research since such an environment is found during the compression phase of the imploding capsule [1]. In addition to laboratory plasmas, strongly coupled systems can be found in the interior of white dwarfs, neutron stars and in other astrophysical environments where the matter is compressed to densities above solid. The understanding of electron transport, recombination dynamics and phase transitions in strongly coupled plasmas poses a challenging theoretical task since the usual expansions of the plasma kinetic equations with respect to the plasma parameter are not applicable [2]. On the other hand, the benchmarking of theoretical models has been mostly limited to comparisons with numerical simulations due to the experimental difficulties in creating strongly coupled plasma conditions in a controlled laboratory environment. Recently, attempts have been made to create strongly coupled plasmas in the laboratory: for example, using sub-picosecond laser pulse irradiation of very thin aluminum foils in order to investigate recombination dynamics in highly transient plasmas [3]. Eidmann *et al.* [4] have also presented a spectroscopical characterization of a solid density strongly coupled Al plasma inferred from He-like and Li-like satellites. On the other hand, since opacity effects can be important during the transport of such lines outside the plasma, the interpretation of the experimental results may depend on the details of the atomic model. Despite these efforts, the exact microscopic characterization of strongly coupled plasmas relies heavily on accurate ionization balance measurements of both the electron temperature ( $T_e$ ), the electron density ( $n_e$ ) and the average charge state ( $Z$ ). Novel experiments based on the analysis of the energy resolved x-ray scattering spectra from solid density plasmas produced by nanosecond laser pulses [5, 6] have proven very successful in the characterization of such systems and providing the test-bed for the validation of dense matter codes.

The degree of Coulomb coupling between charged particles of species  $a$  and  $b$  (where  $a, b = e, i$ , for electrons and ions, respectively) is usually described by the parameter [7]  $\Gamma_{ab} = Z_a Z_b e^2 / 4\pi\epsilon_0 k_B \tilde{T}_e d_{ab}$ , where  $Z_a$  and  $Z_b$  are the respective electrical charges,  $\tilde{T}_e$  is the effective electron temperature [8], and  $d_{ab} = [3(Z_a Z_b)^{1/2} / 4\pi n_e]^{1/3}$  is their average separation. In the case of a classical plasma, the electron kinetic temperature is much larger than the Fermi energy of the electrons,  $T_e \gg T_F$ , thus  $\tilde{T}_e \approx T_e$ . In the opposite regime of a degenerate plasma,  $\tilde{T}_e \approx T_F$ . For our experimental conditions,  $T_F \sim 25$ -40 eV while  $T_e \gtrsim 60$ -100 eV, thus the plasma is essentially classical. Strongly coupled plasma regimes are defined by the condition  $\Gamma_{ab} \gtrsim 1$ . While strong electron-electron

\* Corresponding author: e-mail: gregori1@llnl.gov

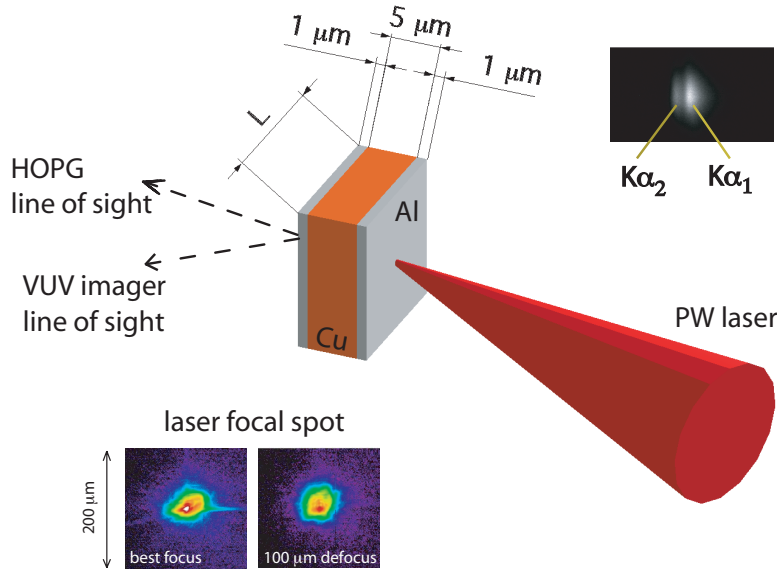


**Fig. 1** (color) Experimental setup showing the multi-layered flat foil, the PW laser incidence, the x-ray spectrometer (HOPG) line of sight and the vacuum ultra-violet (VUV) imager line of sight. The upper inset shows the  $K\alpha$  spectrum recorded on the image plate for a laser energy  $E_L = 11$  J and intensity  $I = 6.6 \times 10^{18}$  W/cm<sup>2</sup> on a target with  $L = 400$   $\mu$ m. The bottom inset shows the images (log scale) of laser spot at best focus and with 100  $\mu$ m defocus.

coupling ( $\Gamma_{ee} > 1$ ) requires super-solid electron densities or low  $T_e$ , strong ion-ion and ion-electron coupling can be achieved at solid densities due to the scaling dependence of the Coulomb forces with the ionic charge.

At solid densities, kinetic relaxation processes occur on a very short time-scale, thus sub-picosecond, high intensity laser pulses are indeed required for the understanding of highly transient systems. In this work we present an experimental investigation of picosecond laser produced strongly coupled plasmas. Since short-pulse x-ray scattering diagnostics cannot currently be implemented because of the requirement of both a plasma producing and a x-ray backlighter beam, we have developed an alternative diagnostic technique based on spectrally resolved measurements of the inner shell ( $K\alpha$ ) emission from both neutral and multiply ionized species induced by fast electrons traversing the dense plasma. The advantage of this technique relies on the simultaneous generation and probing of a strongly coupled plasma with a single high intensity short-pulse beam illuminating a tampered Cu foil; and, since for our experimental conditions  $K\alpha$  lines are optically thin, we can relax to some extent the dependence on the atomic model. By fitting the measured  $K\alpha$  spectra with a dense plasma code we were able to infer  $T_e$  and  $Z$  for a range of laser illumination as well as demonstrate that we can create a well defined strongly coupled plasma with  $\Gamma_{ii} \gtrsim 8$  and  $\Gamma_{ei} \sim 1$ .

The paper is structured as follows. In section §2 we will present the experimental detail of this work. Section §3 will be devoted to the analysis and the theoretical interpretation of the observed line shapes. Concluding remarks will be drawn in section §4.

## 2 Experiment

The layout of the experimental setup is shown in Fig. 1. We have focused the *Vulcan* Petawatt laser at the Rutherford Appleton Laboratory (UK) onto a square, solid multilayered, flat foil with a 600 mm  $f/3$  off axis parabola at  $\sim 28$  degrees incidence from the foil normal. The laser energy was varied between 10 to 400 J, with pulse duration chosen either at 10 ps or 0.4 ps. The spot size diameter was also varied between 16  $\mu$ m at best focus (with 50% of the laser energy contained in it) and 22  $\mu$ m by moving the target plane 100  $\mu$ m towards the focusing parabola. The spot size, pulse duration and laser energy were varied in order to keep the laser irradiance  $I \sim 10^{18}$ - $10^{19}$  W/cm<sup>2</sup>. The target foil consisted of 5  $\mu$ m Cu sandwiched between 1  $\mu$ m Al on both sides. The

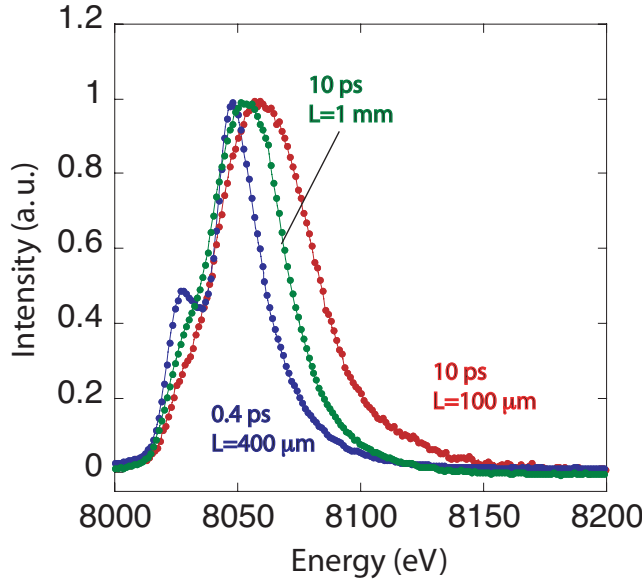


**Fig. 2** (color) Experimental Cu K $\alpha$  profiles: (blue line)  $L = 400 \mu\text{m}$ ,  $E_L = 11 \text{ J}$  and  $I = 6.6 \times 10^{18} \text{ W/cm}^2$ ; (green line)  $L = 1 \text{ mm}$ ,  $E_L = 251 \text{ J}$  and  $I = 3.6 \times 10^{18} \text{ W/cm}^2$ ; (red line)  $L = 100 \mu\text{m}$ ,  $E_L = 259 \text{ J}$  and  $I = 3.7 \times 10^{18} \text{ W/cm}^2$ .

overall mass of the target was also changed by varying the side length ( $L$ ) of the foil from  $100 \mu\text{m}$  to  $1 \text{ mm}$ . From particle-in-cell simulations (PIC), the expected temperature of the hot electrons generated at the foil front surface is  $T^{\text{hot}} = 0.13 I_{17}^{0.5} \approx 0.4\text{-}3.2 \text{ MeV}$ , where  $I_{17}$  is the laser intensity given in units of  $10^{17} \text{ W/cm}^2$  [9]. These multi-keV electrons penetrate the target and generate x rays via K-shell ionization. The number and the duration of x-ray photons produced is a complicated function of the foil thickness. For our experimental conditions, the duration of the primary x-ray K $\alpha$  emission after the end of the laser pulse is from PIC simulations predicted to be  $\sim 95 \text{ fs}$  [9]. As the fast electrons pass through the target, a space charge is created which forces the electrons to re-circulate between the front and the rear surfaces [10, 11]. During each pass, additional K $\alpha$  fluorescence of the copper can be induced, thus extending the overall duration of the x-ray emission up to  $\sim 0.5\text{-}1 \text{ ps}$  after the end of the laser pulse. During this time, the Al tamper is sufficient to prevent hydrodynamic expansion of the Cu foil, thus maintaining solid density condition in the emitting region. This is justified by the fact that the hydrodynamic disruption of the foil will occur on the time-scale dictated by the ion sound speed  $c_s = (ZT_e/M)^{0.5}$ , where  $M$  is the mass of the copper ions, which, for our experimental conditions is found to be  $c_s \approx 0.02\text{-}0.07 \mu\text{m/ps}$ . Thus, substantial expansion of the foil is expected  $\gtrsim 70 \text{ ps}$  after the end of the laser pulse when the K $\alpha$  emission has ceased.

The time and spatially integrated K $\alpha$  radiation emitted by the Cu foil was then spectrally resolved with a high efficiency, sagittally curved highly oriented pyrolytic graphite (HOPG) crystal [12] coupled to an image plate detector [13, 14]. The crystal collected the x rays emitted from the back surface at 42 degrees from the foil normal. Since the optical depth of the cold Cu K $\alpha$  line through the foil is  $\tau_{K\alpha} \lesssim 0.2$ , opacity effects can be neglected and the observed line can be considered optically thin. In addition to the x-ray spectrometer, vacuum ultra violet (VUV) emission at 68 eV from the back surface was also measured as indicated in Fig. 1. The VUV imaging diagnostic consisted of a spherical multilayer mirror set to Bragg reflect back surface thermal emission onto a cooled, 16 bit,  $1024 \times 1024 \text{ CCD}$  with  $5 \mu\text{m}$  pixel resolution [15].

Some of the relevant measured K $\alpha$  spectra are plotted in Fig. 2. At the lowest laser energy on target, we clearly see separation between the copper K $\alpha_1$  and K $\alpha_2$  doublet, thus providing an accurate dispersion calibration of our data. The error in absolute wavelength position between different spectra is estimated to be  $\sim 3\text{-}4 \text{ eV}$ . Since the

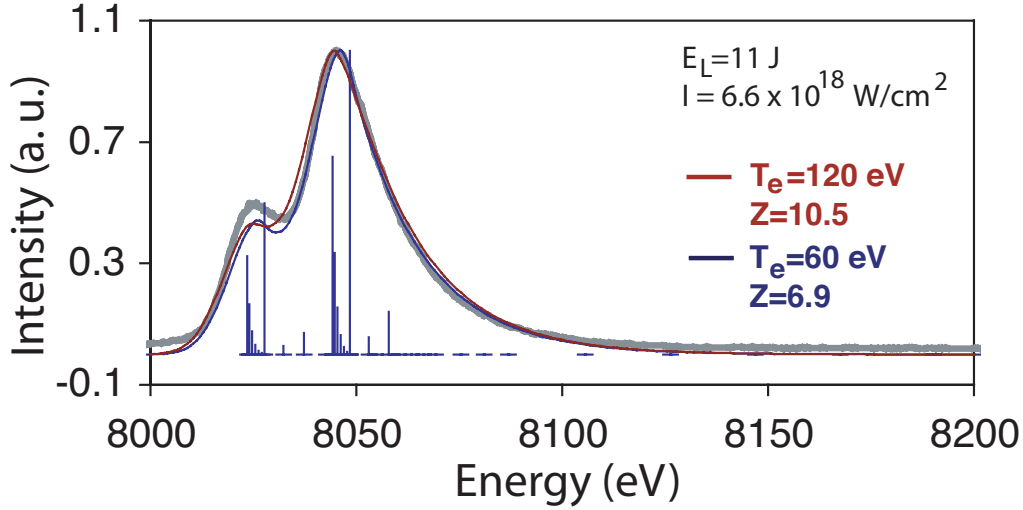


**Fig. 3** (color) Measured spectrum at low laser energy (gray line) compared with synthetic from the average atom model muZe with the corresponding best fit values for electron temperature ( $T_e$ ) and average ionization state ( $Z$ ). Individual lines corresponding to various ionization stages at  $T_e = 60$  eV and  $Z = 6.9$  are plotted. These data were obtained by driving the foil with a 0.4 ps laser pulse on a  $L=400$   $\mu\text{m}$  target. Laser energy ( $E_L$ ) and intensity are given in the figure for both shots.

HOPG is operated in mosaic focussing mode, the high energy side of the experimental line is instrumentally broadened by volume diffraction underneath the crystal surface [16], which we include in our analysis. In this respect, we should point out that the measured line shape at low laser energy is mainly determined by this asymmetric instrument function. As the laser energy is increased, from Fig. 2, we observe a substantial broadening and wavelength shift of the measured spectral lines towards the higher energies, indicating that a large fraction of the  $K\alpha$  radiation is emitted by highly ionized atoms [17, 18], which also suggests plasma conditions with higher  $T_e$ . Since the Cu foil is tamped by Al on both sides, bulk hydrodynamic motion cannot occur during the times the  $K\alpha$  radiation is emitted, thus Doppler shifts from plasma expansion cannot explain the observed blue wing of the line. Doppler broadening of the measured lines is estimated as  $\Delta E_d = 2E_{K\alpha} \sqrt{2(\ln 2)k_B T_e / M c^2} \approx 1.1$  eV at  $T_e \sim 200$  eV, where  $E_{K\alpha} = 8.0$  keV,  $M$  is the Cu mass, and  $c$  is the speed of light, thus it only accounts for a small fraction of the observed line width. The collisional dissipation of the fast electrons, which are confined within the target by the Debye sheath, or the return current of the slower electrons volumetrically heat the foil. Since the conversion of laser energy into hot electrons is roughly constant over the intensity range considered in our experiment [9], smaller mass targets (*i.e.*, smaller  $L$ ) are expected to achieve higher temperatures since an equal amount of energy is deposited in a smaller volume. This effect is indeed visible from Fig. 2, where at comparable laser energies on target, the foil with smaller mass show a more pronounced blue wing, and likely higher electron temperatures. At the same time, direct heating of the copper foil from VUV and soft x-ray radiation from the hot front surface is largely prevented by the Al tamper, thus leaving ohmic dissipation as the dominant heating mechanism.

### 3 Analysis and discussion of the results

As mentioned earlier,  $K\alpha$  radiation freely escapes the dense plasma without coupling with the matter [19], and this considerably simplifies the analysis of the experimental spectra. While measurements of  $K\alpha$  yields have been shown a powerful diagnostics in determining hot electron temperatures [20, 21, 22, 23], analysis of the spectral distribution of the  $K\alpha$  emission from multiply ionized atoms may be applied to determining the ionization balance of the dense plasma. In particular, as shown by Chen *et al.* [21], the return current from hot electrons can preheat Al/Si layered foils up to  $\sim 100$  eV, thus significant ionization of the dense plasma may occur.

In order to extract the dense Cu ionization balance from the experimental spectra, a self-consistent-field model of ions in dense plasmas (muZe) was used [24]. The model starts from self-consistent Thomas-Fermi electron

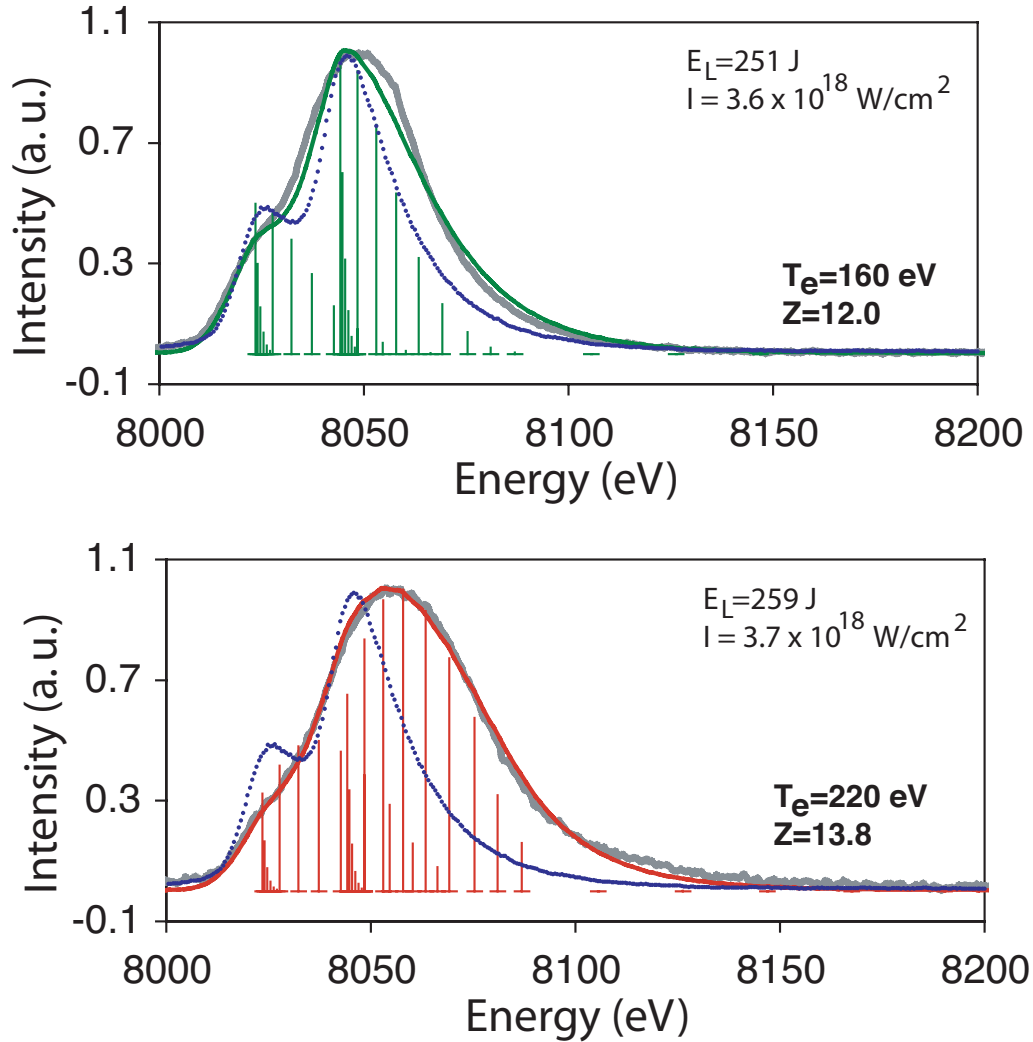


**Fig. 4** (color) Top: Experimental spectrum for a  $L=1$  mm target (gray line) and best fit (green line) from the average atom model muZe. Individual lines for the various ionization stages are also plotted. Bottom: Experimental spectrum for a  $L=100$   $\mu\text{m}$  target (gray line) and best fit (red line) from the average atom model muZe. Individual lines for the various ionization stages are also plotted. These data were obtained by driving the foil with a 10 ps laser pulse. Best fit values for electron temperature ( $T_e$ ) and average ionization state ( $Z$ ) are also indicated in the plots. The *cold*  $K\alpha$  spectrum from Fig. 3 is given (blue dots) as reference.

density and potential in a Wigner-Seitz cell whose radius is determined by the ion density. As discussed previously, the Al tamper prevents the expansion of the Cu during the time the  $K\alpha$  lines are emitted, thus the ion density is given by its solid value  $n_i = 8.5 \times 10^{22} \text{ cm}^{-3}$ . Non-relativistic bound and free wavefunctions are calculated in this initial potential with the chemical potential chosen in order to preserve charge neutrality. A new electron density is thus determined and a corresponding potential is obtained from Poisson's equation. Exchange and correlation effects are then added to this potential following the approach suggested by Rozsnyai [25]. This procedure is repeated iteratively until convergence is reached, giving self-consistent values for the chemical potential and the average charge state,  $Z$ . The average atom model is then split into individual ions, with potentials and wavefunctions optimized for each ion within the Wigner-Seitz cell so that continuum lowering is automatically accounted for. Relativistic corrections are added to the bound state energies (thus accounting for the  $K\alpha_1$  and  $K\alpha_2$  splitting) and a single global correction is added to the calculated transition energies so that the cold

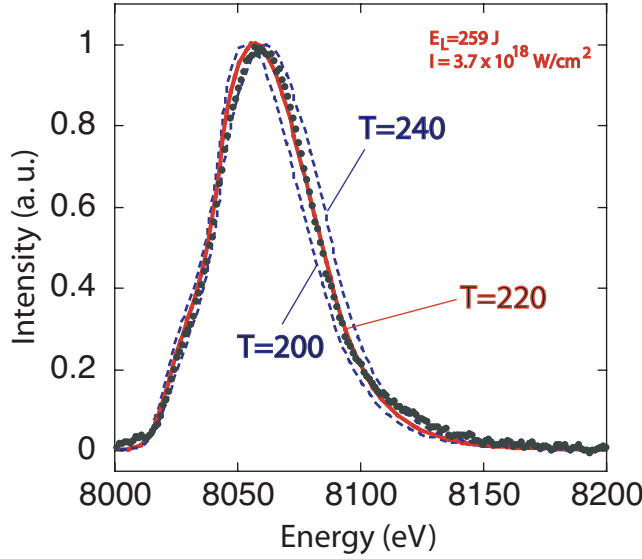


**Fig. 5** (color) Sensitivity analysis for the electron temperature best fit from case (e) in Fig. 4. The experimental line shape is plotted against the best fit and other two synthetic spectra obtained by varying  $T_e$  by 20 eV.

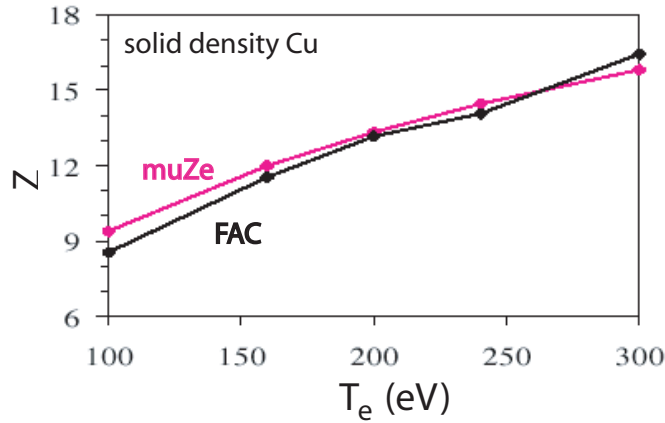


**Fig. 6** (color) Predicted ionization state ( $Z$ ) for solid density copper as a function of the electron temperature ( $T_e$ ) for both FAC and muZe.

$K\alpha$  line matches the tabulated values [26]. Once the transition energies are calculated, oscillators strengths and population densities are obtained within Saha-Boltzmann equilibrium. We should point out that at solid densities, local thermodynamic equilibrium (LTE) is closely approached [27] due to fast collisional relaxation. Finally, synthetic spectra are constructed and convoluted with the experimental instrumental response.

The experimental spectrum obtained by driving the foil at low laser energy ( $E_L = 11$  J), with a 0.4 ps laser pulse on a  $L=400$   $\mu\text{m}$  target is given in Fig. 3 together with two different synthetic spectra calculated by muZe: one at  $T_e = 60$  eV and  $Z = 6.9$  and the other at  $T_e = 120$  eV and  $Z = 10.5$ . For both cases, differences between the experimental and the calculated line shapes are minimal, suggesting that the observed spectral shape is mainly determined by the instrument response. This provides a lower bound to the sensitivity in the electron temperature

and ionization state. As the laser energy is increased (see Fig. 4), while keeping the laser intensity approximately constant by stretching the laser pulse to 10 ps, ohmic heating becomes progressively more important and a large fraction of  $K\alpha$  is emitted by multiply ionized atoms. This effect is clearly visible in Fig. 4 with the merging of the  $K\alpha_1$  and  $K\alpha_2$  doublet due to the blue shift in the inner shell emission lines of higher ionization stages which results into a broadened experimental spectrum. The experimental data are thus a direct evidence of increased ionization in Copper. By comparison with muZe, at the highest laser energies,  $Z$  reaches  $\sim 14$  and the inferred  $T_e$  exceeds 200 eV.

The precision of the inferred  $T_e$  and  $Z$  depends on both on the accuracy of the fitting procedure as well the validity of atomic model used to construct the synthetic line profiles. As an example, Fig. 5 shows the temperature sensitivity of the fitting procedure, which we use to infer an error in  $T_e$  on the order of  $\pm 20$  eV. Similarly, we can assess that the fitting error in  $Z$  is  $\lesssim \pm 1$ . To test the accuracy of muZe, we have compared our results to atomic structure calculations from the relativistic multiconfiguration atomic code FAC [28, 29]. FAC predicts many hundreds of lines for each ion, but the dominant emission feature generally retains the dual peak shape of the characteristic  $K\alpha$  lines. Since those fine details of the spectrum are not resolved by our instrument, FAC and muZe indeed show very similar  $K\alpha$  emission characteristics. The predicted ionization state as a function of  $T_e$  from the two codes at solid density is plotted in Fig. 6. We see that the overall accuracy in  $Z$  is  $\pm 1$ , while the corresponding error in  $T_e$  is  $\pm 45$  eV. Based on these considerations, we can estimate a cumulative error  $\Delta T_e = \pm 50$  eV and  $\Delta Z = \pm 1.4$ .

A final point on the validity of this analysis relates on the interpretation of time integrated and spatially integrated spectra. As we have mentioned,  $K\alpha$  emission will probably last up to  $\sim 0.5$ -1 ps after the end of the main laser pulse, including the effects of electron refluxing. Thus, particularly for the 10 ps pulse, the  $K\alpha$  emission mostly occurs while the laser is on, and, this is also the time during which the heating of the target takes place. In this respect, our measurements are representative of the average temperatures and ionization state during the heating phase of the solid density plasma, but they are not representative of the subsequent cooling by thermal conduction and radiation transport. Assuming a linear increase of the electron temperature during the heating phase, we can expect peak temperatures about two times higher than the average ones. Spatial gradients in  $T_e$  and  $Z$  across the foil may also be present, due to the fact that the conversion of laser energy into fast electrons occurs on a very small spatial scale, at the laser spot, which for our experiments was varied between 18-22  $\mu\text{m}$ . However, since heating is carried by these MeV electrons, their mean free path through the solid matter is comparable or longer than the dimension of the foil, thus volumetric and isochoric heating is expected. This is elucidated in Fig. 7 which shows the measured, temporally integrated, spatial distribution of the VUV emission at 68 eV from the back surface of the target. From the figure we see a factor  $\sim 2$  in the spatial variation of the intensity distribution at the rear surface. Assuming, roughly, that the back surface is a uniform gray-body emitter, such a change in intensity corresponds to a variation in the temperature distribution across the surface of  $\lesssim 20\%$ , which is within the experimental uncertainties of our measurements.

Another point which is evident from Fig. 4 is that, at comparable laser energies, the low mass target ( $L=100 \mu\text{m}$ ) show higher temperature than higher mass one ( $L=1 \text{ mm}$ ). We have previously interpreted this effect as a result of the fast electrons being constrained by the space charge, thus effectively depositing a similar amount of energy (for comparable laser intensities) into a smaller volume. Such an increase in energy density is expected then to results in a higher ionization of copper and consequently higher electron temperatures. In order to show such a dependence of electron heating on both laser energy and mass, we have illuminated targets with  $L=100 \mu\text{m}$  and  $L=1 \text{ mm}$  over a range of the laser energies. The results are illustrated in the plots of Fig. 9 and Fig. 8 that show the inferred average ionization and electron temperature, respectively, as a function of the energy density deposited on the foil during the laser pulse.

our work shows that a relatively large range of solid density plasma conditions can be achieved. In particular, while the ion-ion coupling constant  $\Gamma_{ii} = 8$ -9 for all the experimental conditions investigated in this study, the electron-ion and the electron-electron coupling parameters show a larger range of variations:  $\Gamma_{ei} = 1$ -1.6,  $\Gamma_{ee} = 0.1$ -0.3. These plasma conditions are also relatively well defined in our experiment, as the degree of heating is directly related to the mass of the target, and they could provide a diagnostics platform for the validation of optical properties and structure dynamics in strongly coupled systems [30, 31, 32].

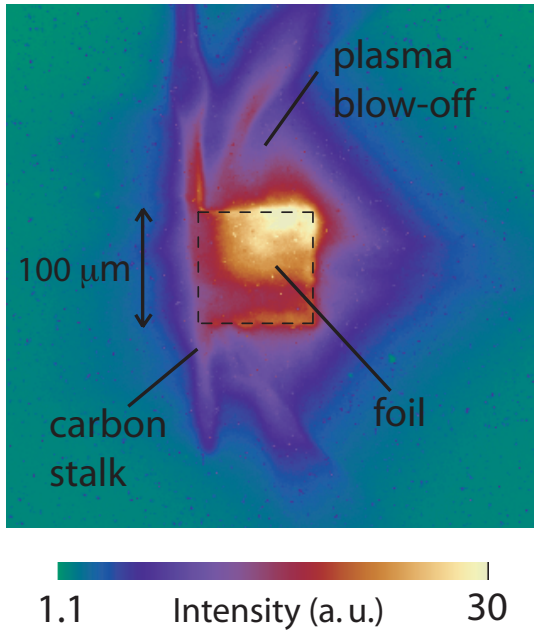


**Fig. 7** (color) VUV image at 68 eV of the rear surface of the foil. The data was obtained with a  $L=100\ \mu\text{m}$  foil, with laser energy  $E_L = 390\ \text{J}$  and intensity  $I = 9.7 \times 10^{18}\ \text{W}/\text{cm}^2$ . Low density plasma blow-off from the front surface of the target is also seen around the foil.

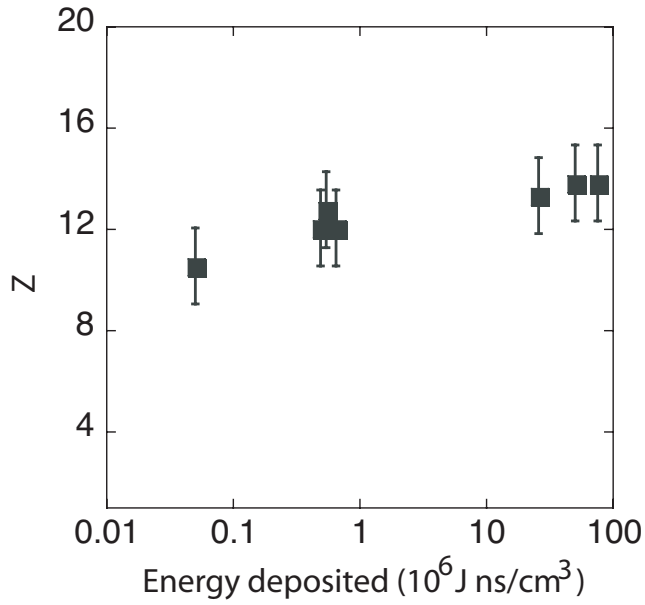


**Fig. 8** Average ionization vs energy density deposited on the target during the laser pulse.

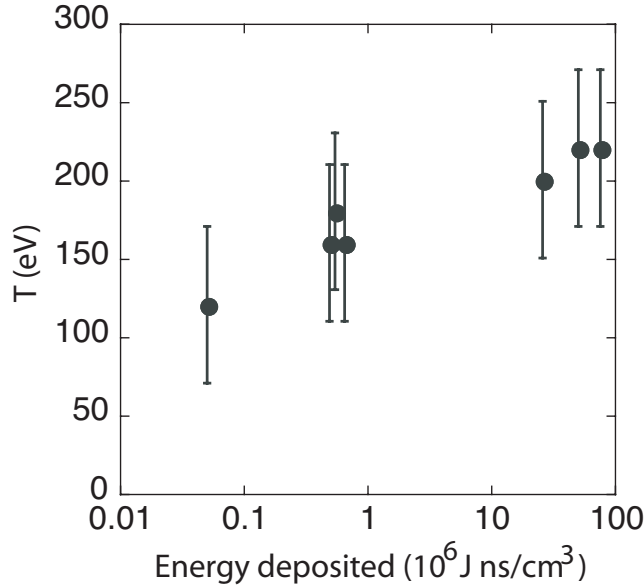


**Fig. 9** Electron temperature vs energy density deposited on the target during the laser pulse.

#### 4 Concluding remarks

We have shown that by using an intense laser, a buried Cu foil can be heated up to few hundred electron-volts with average ionization state  $Z = 13$ -14, achieving strongly coupled plasma conditions at solid density. The plasma was diagnosed by obtaining time and spatially integrated spectra of the  $K\alpha$  fluorescence of the copper atoms induced by the fast electrons, produced at the front of the target, as they traverse the foil. In order to infer temperature and ionization state of the copper material during the heating, the measured Cu spectra have been fitted with a self-consistent-field for ions in dense plasmas. Comparison with a fully relativistic multi-configuration atomic structure code showed that the cumulative error in the measured  $T_e$  is  $\pm 50$  eV and in the average  $Z$  is  $\pm 1.4$ . These type of plasma could provide a laboratory test bed for the accurate validation of solid density electron transport codes, relevant to ICF research, as well as for the understanding of the optical response of strongly coupled systems. In particular, since opacity can be neglected, copper doped CD capsules could be proposed for the measurement of the electron temperature during the implosion phase in fast ignition experiments driven by either fast electrons or protons [33, 34].

**Acknowledgements** This work was part of a large international collaboration. The authors would like to thank D. Hey, N. Izumi, N. Patel, and B. Zhang (Lawrence Livermore National Laboratory), R. Freeman (Ohio State University), R. Stephens (General Atomics), and W. Theobald (University of Rochester). The experimental support of R. Clark and R. Heathcote at the Rutherford Appleton Laboratory is also acknowledge. The work described in this paper was performed under the auspices of the U.S. Department of Energy by the University of California Lawrence Livermore National Laboratory under Contract No. W-7405-ENG-48.

## References

- [1] J. D. Lindl. *Inertial Confinement Fusion*. Springer-Verlag, New York, 1998.
- [2] S. Ichimaru. *Basic Principles of Plasma Physics*. Addison, Reading, MA, 1973.
- [3] P. Audebert, P. Renaudin, S. Bastiani-Ceccotti, J.-P. Geindre, C. Chenais-Popovics, A. Tzortzakis, V. Nagel-Silvert, R. Shepherd, I. Matsushima, S. Gary, F. Girard, O. Peyrusse, and J.-C. Gauthier. *Phys. Rev. Lett.*, 94:025004, 2005.
- [4] K. Eidmann, A. Saemann, U. Andiel, I. E. Golovkin, R. C. Mancini, E. Andersson, and E. Förster. *J. Quant. Spectrosc. Radiat. Transfer*, 65:173, 2000.
- [5] S. H. Glenzer, G. Gregori, R. W. Lee, F. J. Rogers, S. W. Pollaine, and O. L. Landen. *Phys. Rev. Lett.*, 90:175002, 2003.
- [6] S. H. Glenzer, G. Gregori, F. J. Rogers, D. H. Froula, S. W. Pollaine, R. S. Wallace, and O. L. Landen. *Phys. Plasmas*, 10:2433, 2003.
- [7] S. Ichimaru. *Rev. Mod. Phys.*, 54:1017, 1982.
- [8] G. Gregori, S. H. Glenzer, W. Rozmus, R. W. Lee, and O. L. Landen. *Phys. Rev. E*, 67:026412, 2003.
- [9] Ch. Reich, P. Gibbon, I. Uschmann, and E. Förster. *Phys. Rev. Lett.*, 84:4846, 2000.
- [10] Y. Sentoku, T. E. Cowan, A. Kemp, and H. Ruhl. *Phys. Plasmas*, 10:2009, 2003.
- [11] A. J. Mackinnon *et al.* *Phys. Rev. Lett.*, 88:215006, 2002.
- [12] M. K. Urry, G. Gregori, O. L. Landen, A. Pak, and S. H. Glenzer. *J. Quant. Spectrosc. Radiat. Transfer*, submitted, 2005.
- [13] J. Miyahara, K. Takahashi, Y. Amemiya, N. Kamiya, and Y. Satow. *Nucl. Instrum. Methods Phys. Res.*, A246:572, 1986.
- [14] Y. Amemiya, T. Matsushita, A. Nakagawa, Y. Satow, J. Miyahara, and J. Chikawa. *Nucl. Instrum. Methods Phys. Res.*, A266:645, 1988.
- [15] M. H. Key *et al.* In K.A. Tanaka, D.D. Meyerhofer, and J. Meyer ter Vehn, editors, *Inertial Fusion Sciences Applications*, page 357. Elsevier, Paris, 2002.
- [16] A. Pak, G. Gregori, J. Knight, K. Campbell, D. Price, B. Hammel, O. L. Landen, and S. H. Glenzer. *Rev. Sci. Instrum.*, 75:3747, 2004.
- [17] U. Andiel, K. Eidmann, P. Hakel, R. C. Mancini, G. C. Junkel-Vives, J. Abdallah, and K. Witte. *Europhys. Lett.*, 60:861, 2002.
- [18] H. Nishimura, T. Kawamura, R. Matsui, Y. Ochi, S. Okihara, S. Sakabe, F. Koibe and T. Johzaki, H. Nagamoto, K. Mima, I. Uschmann, and E. Forster. *J. Quant. Spectrosc. Radiat. Transfer*, 81:327, 2003.
- [19] D. Duston, R. W. Clark, J. Davis, and J. P. Apruzese. *Phys. Rev. A*, 27:1441, 1983.
- [20] J. D. Hares, J. D. Kilkenny, M. H. Key, and J. G. Lunney. *Phys. Rev. Lett.*, 42:1216, 1979.
- [21] H. Chen, B. Soom, B. Yaakobi, S. Uchida, and D. D. Meyerhofer. *Phys. Rev. Lett.*, 70:3431, 1993.
- [22] U. Tuebner *et al.* *Phys. Rev. E*, 54:4167, 1996.
- [23] R. W. Stephens *et al.* *Phys. Rev. E*, 69:066414, 2004.

- [24] S. B. Hansen, A. Ya. Faenov, T. A. Pikuz, K. B. Fournier, R. Shepherd, H. Chen, J. R. Hunter, Y. Ping, K. Widmann, S. Wilks, G. Dyer, and T. Ditmire. *Phys. Rev. E*, 2005.
- [25] B. Rozsnyai. *Phys. Rev. A*, 58:1137, 1972.
- [26] J. A. Bearden. *Rev. Mod. Phys.*, 39:78, 1967.
- [27] D. Duston and J. Davis. *Phys. Rev. A*, 21:1664, 1980.
- [28] M. F. Gu. *Astrophys. J*, 590:1131, 2003.
- [29] M. F. Gu. *Astrophys. J*, 582:1241, 2003.
- [30] J.-P. Hansen and I. R. McDonald. *Phys. Rev. A*, 23:2041, 1981.
- [31] R. Cauble and D. B. Boercker. *Phys. Rev. A*, 28:944, 1983.
- [32] D. B. Boercker, R. W. Lee, and F. J. Rogers. *J. Phys. B*, 16:3279, 1983.
- [33] M. Tabak *et al.* *Phys. Plasmas*, 1:1626, 1994.
- [34] R. Kodama, P. A. Norreys, K. Mima, A. E. Dangor, R. G. Evans, H. Fujita, Y. Kitagawa, K. Krushelnick, T. Miyakoshi, N. Miyanaga, T. Norimatsu, S. J. Rose, T. Shozaki, K. Shigemori, A. Sunahara, M. Tampo, K. A. Tanaka, Y. Toyama, T. Yamanaka, and M. Zepf. *Nature*, 412:798, 2001.